2019 SCEC Annual Report

Implementation of Inter-frequency-spatial Ground Motion Correlation in the SDSU BBP Module

Report for SCEC Award 19130

PI: Dr. Kim B. Olsen

Institution: Department of Geological Sciences, San Diego State University, San Diego, CA 92182-1020

Publications and Reports:

Wang, N., K.B. Olsen, and S.M. Day (2020). A Frequency-Dependent Ground-Motion Spatial Correlation Model of Within-Event Residuals for Fourier Amplitude Spectra, submitted to *Earthquake Spectra.*

Wang, N., R. Takedatsu, K.B. Olsen, and S.M. Day (2019). Inclusion of Frequency-Dependent Spatial Correlation into the SDSU Broadband Ground-Motion Generation Method, *SCEC Annual Mtg*, September 7-11, Palm Springs, CA, Poster #014.

Recorded Zoom presentation by Nan Wang (3/18/2020):

https://sdsu.zoom.us/rec/play/vsYtlumtrDo3SNKS5gSDVv96W9S9ev6s1yMX_aULyhy0UnVSYQKvZ-ZBNLBp1O-sItfXUnqLXwaPDY2J?autoplay=true&startTime=1584569063000

Summary

Ground motion time series recorded at stations separated by up to about 50 kilometers show a frequency-dependent spatial coherency structure, and the corresponding ground motion intensity measures are found to be correlated. As omitting this correlation can result in underestimation of seismic losses in risk analysis, it is critical to quantify the spatial correlation structure for ground motion Fourier spectra estimated at different sites during a single event within a region. Toward this goal, we have developed an empirical frequency-dependent spatial correlation model for the within-event residuals of effective Fourier amplitude spectra from the Pacific Earthquake Engineering Research Center (PEER) Next Generation Attenuation (NGA) West2 database. The correlation model shows slower decrease of the spatial correlation with distance at lower frequencies as compared to higher frequencies, in agreement with the underlying ground motion data, and no significant dependence on the magnitude of the earthquakes is observed. We use this empirical model to incorporate frequency-dependent spatial correlation into a hybrid deterministic-stochastic broadband ground motion generation module, which successfully generates synthetic time series for 7 western U.S. earthquakes with frequency-dependent spatial correlation that closely mimics that of the empirical model. Furthermore, the method also significantly improves the correlation for spectral accelerations, Cumulative Absolute Velocities (CAVs), and Arias Intensities (AIs) compared with that derived from the original broadband module.

Within-Event Residual of the Effective Amplitude Spectrum

FAS, the amplitude spectrum of Fourier transform of the acceleration time series, depends on the recording instrument's orientation. Such dependency may cause an undesirable bias in applications of the calculated FAS values. On the other hand, the EAS defined by Goulet *et al.* (2018) as

$$EAS(f) = \sqrt{\frac{1}{2}\left[FAS_{HC1}^2(f) + FAS_{HC2}^2(f)\right]} \qquad \text{Eq. 1}$$

is rotation independent, and will therefore be used as the intensity measure for our empirical model development. As discussed later, we then use the EAS model, with the method of Wang et al. (2019), to generate FAS adjustments to simulated time histories. In Equation 1, FAS_{HC1} and FAS_{HC2} are the FAS of two orthogonal as-recorded horizontal components acceleration time series, and f is the frequency in Hertz. The EAS is smoothed by the $\log_{10}$-scale Konno and Ohmachi (1998) smoothing window (e.g., Kottke *et al.*, 2018):

$$W(f) = \left(\frac{\sin\left(b\log(f/f_c)\right)}{b\log(f/f_c)}\right)^4. \qquad \text{Eq. 2}$$

Here, W is a weight at frequency f designed for a window with center frequency f_c, and $b = \frac{2\pi}{b_w} = 60\pi$, where b_w is the smoothing window bandwidth in $\log_{10}$ units (see Kottke *et al.* (2018) for more details on the smoothing technique).

The normalized EAS within-event residual, epsilon (ε), at station s during earthquake e is calculated as a function of frequency f as:

$$\varepsilon(f) = \frac{\delta W_{es}(f)}{\varphi(f)} = \frac{\ln EAS_{es}(f) - \mu_{\ln EAS_{es}}(f) - \delta B_e}{\varphi(f)}, \qquad \text{Eq. 3}$$

where φ is the standard deviation, and epsilon is standard normally distributed.

Semivariogram Analysis

A semivariogram (γ) characterizes the strength of statistical dissimilarity as a function of distance and is often used to describe spatially distributed random variables in geostatistics**.** The empirical semivariogram matrix for ε at each frequency pair (f_i, f_j) can be summarized by an isotropic semivariogram matrix (Γ) as a function of separation distance h:

$$\Gamma(h) = \gamma_{f_i,f_j}(h) = \begin{bmatrix} \gamma_{f_1,f_1}(h) & \cdots & \gamma_{f_1,f_n}(h) \\ \vdots & \ddots & \vdots \\ \gamma_{f_n,f_1}(h) & \cdots & \gamma_{f_n,f_n}(h) \end{bmatrix}, \qquad \text{Eq. 4}$$

where matrix element γ_{f_i,f_j} is as defined, in terms of epsilon. Similarly, the empirical isotropic covariance matrix (C) can be written as a function of separation distance h as:

$$\mathrm{C}(h) = c_{f_i,f_j}(h) = \begin{bmatrix} c_{f_1,f_1}(h) & \cdots & c_{f_1,f_n}(h) \\ \vdots & \ddots & \vdots \\ c_{f_n,f_1}(h) & \cdots & c_{f_n,f_n}(h) \end{bmatrix}, \qquad \text{Eq. 5}$$

and we have

$$C(h) = C(0) - \Gamma(h). \qquad \text{Eq. 6.}$$

Data Sources

In this study, the frequency-dependent spatial correlation model is developed from EAS values for recorded ground motions in the PEER NGA West2 database (Ancheta et al., 2014). The NGA-West2 database includes shallow crustal earthquakes with M>3 in active tectonic regions. The normalized within-event EAS residual, epsilon, was determined from the Bayless and Abrahamson (2018b) model. This model was calculated from the individual EAS values and the earthquake-specific smoothed EAS median model for each recorded event at each station. For more details on the ground-motion database and data selection criteria, see Bayless and Abrahamson (2018b) and Abrahamson et al. (2014).

Semivariograms γ_{f_i,f_j} of epsilon were calculated for each pair of frequencies, f_i and f_j (at frequency points 0.1-1 Hz with a spacing of 0.1 Hz, and 1-23 Hz with a spacing of 1 Hz) and as a function of h from 0 to 120 km with a bin size equal to 2 km.

Linear Model of Coregionalization

Previous studies (e.g. Wang and Takada, 2005) have observed an exponential decay of the ground motion spatial correlation, suggesting that the semivariogram can be well fit using an exponential model. For this reason, we anticipate fitting the semivariogram to a function with the general behavior:

$$\gamma(h) = S\left[1 - \exp\left(-\frac{3h}{R}\right)\right], \qquad \text{Eq. 7}$$

where S is the sill that represents the asymptotic value of $\gamma(h)$ as h goes to infinity, and R is the range that represents the distance at which the value of $\gamma(h)$ equals 95% of the sill. In the multivariate case, this general behavior would imply a semivariogram at a given frequency pair f_i and f_j of the form:

$$\gamma_{ij}(h) = S_{ij}\left[1 - \exp\left(-\frac{3h}{R_{ij}}\right)\right]. \qquad \text{Eq. 8}$$

However, it has been shown that (for within-event residuals of spectral accelerations) R_{ij} varies at different frequencies such that lower frequencies tend to have larger ranges than do higher frequencies (Loth and Baker, 2013). To better represent these frequency dependencies, we followed an approach similar to that of Loth and Baker (2013), using a nested semivariogram model (a linear combination of single semivariogram models):

$$\gamma_{ij}(h) = P_{ij}^1\left(1 - \exp\left(-\frac{3h}{R_1}\right)\right) + P_{ij}^2\left(1 - \exp\left(-\frac{3h}{R_2}\right)\right) + P_{ij}^3. \qquad \text{Eq. 9}$$

Combining all elements γ_{ij}, we obtain the linear model of coregionalization:

$$\Gamma(h) = \boldsymbol{P^1}\left(1 - \exp\left(-\frac{3h}{R_1}\right)\right) + \boldsymbol{P^2}\left(1 - \exp\left(-\frac{3h}{R_2}\right)\right) + \boldsymbol{P^3}, \qquad \text{Eq. 10}$$

where $\boldsymbol{P^1}$ and $\boldsymbol{P^2}$ are coregionalization matrices corresponding to the short-range and long-range models, respectively. Note that the third term, the coregionalization matrix $\boldsymbol{P^3}$ in Equation 10 corresponds to the nugget effect,

$$\gamma(h) = \begin{cases} 0 & if\ h = 0 \\ S & if\ h > 0 \end{cases}, \qquad \text{Eq. 11}$$

which can be used to represent discontinuity of the semivariogram at separation distances larger than zero. Ranges $R_1 = 10$ km and $R_2 = 100$ km provide a reasonable fit to the data and are adopted in our model. The coregionalization matrices, $\boldsymbol{P^1}$, $\boldsymbol{P^2}$ and $\boldsymbol{P^3}$, which are symmetric and semipositive definite, are estimated from the empirical semivariogram data by the procedure given in the next section.

Empirical Frequency-Dependent Spatial Correlation Model for Covariance

We use the Goulard-Voltz algorithm (Goulard and Voltz, 1992) to develop our frequency-dependent spatial correlation model for covariance. The iterative algorithm uses a least square fitting technique to find the coregionalization matrices that minimize the weighted sum of squares:

$$WSS = \sum_{k=1}^{K} \omega_k \left\| \hat{\Gamma}(h_k) - \Gamma(h_k) \right\|^2 = \sum_{k=1}^{K} \omega_k \sum_{i,j=1}^{N} \left[\hat{\gamma}_{ij}(h_k) - \gamma_{ij}(h_k)\right]^2, \qquad \text{Eq. 12}$$

where $\hat{\Gamma}(h_k)$ and $\hat{\gamma}_{ij}(h_k)$ represent the semivariogram values computed from the model, and $\Gamma(h_k)$ or $\gamma_{ij}(h_k)$ represent the semivariogram values computed from the empirical data at h_k, the center of the kth bin. ω_k is a positive weight at h_k, which is defined as $\omega_k = \frac{1}{h_k}$ in this study.

Let us denote $\left(1-\exp\left(-\frac{3h}{R_1}\right)\right)$ by $g^1(h)$, $\left(1-\exp\left(-\frac{3h}{R_2}\right)\right)$ by $g^2(h)$ and 1 by $g^3(h)$. Equation 10 can then be written as:

$$\Gamma(h)=\sum_{l=1}^{L}\boldsymbol{P^l}g^l(h)\ ,\ L=3\ . \qquad \text{Eq. 13}$$

The Goulard-Voltz algorithm is now executed using the following steps:

(1) Initialize the coregionalization matrices $\boldsymbol{P^l}$, $l=1,2,3$ in this study.
(2) Iterate from (a) to (c):
  (a) Compute WSS with the current coregionalization matrices.
  (b) For each l:
    (b1) Compute the new coregionalization matrix $\widetilde{\boldsymbol{P}}^{\boldsymbol{l}}$ as:

$$\widetilde{\boldsymbol{P}}^{\boldsymbol{l}}=\frac{\sum_{k=1}^{K}\omega_k g^l(h_k)\left[\hat{\Gamma}(h_k)-\sum_{u=1,u\neq l}^{L}\boldsymbol{P^u}g^u(h_k)\right]}{\sum_{k=1}^{K}\omega_k\left[g^l(h_k)\right]^2} \qquad \text{Eq. 14}$$

    (b2) Decompose $\widetilde{\boldsymbol{P}}^{\boldsymbol{l}}$ as: $\widetilde{\boldsymbol{P}}^{\boldsymbol{l}}=\boldsymbol{Q_l\Lambda_l Q_l^T}$
      where $\boldsymbol{Q_l Q_l^T}$ is an identity matrix and $\boldsymbol{\Lambda_l}$ is a diagonal matrix.
    (b3) Change all the negative diagonal elements of $\boldsymbol{\Lambda_l}$ to zero to obtain $\boldsymbol{\Lambda_l^+}$ (this step is applied for ensuring semipositive definiteness of each coregionalization matrix).
    (b4) Update $\widetilde{\boldsymbol{P}}^{\boldsymbol{l}}$ as a semipositive definite matrix $\widetilde{\boldsymbol{P}}^{\boldsymbol{l}}=\boldsymbol{Q_l\Lambda_l^+ Q_l^T}$.
  (c) Compute WSS with the updated coregionalization matrices and loop over (a) to (c) until the difference of the WSS value from (a) and (c) is smaller than a positive prespecified value.

Noting that

$$C(0)=\lim_{h\to+\infty}\Gamma(h)=\boldsymbol{P^1}+\boldsymbol{P^2}+\boldsymbol{P^3}, \qquad \text{Eq. 15}$$

the correlation matrix in Equation 5 can be derived from Equation 6 as:

$$C(h)=\boldsymbol{P^1}\exp\left(-\frac{3h}{R_1}\right)+\boldsymbol{P^2}\exp\left(-\frac{3h}{R_2}\right)+\boldsymbol{P^3}I_{\{h=0\}}\ , \qquad \text{Eq. 16}$$

where

$$I_{\{h=0\}}=\begin{cases}1 & h=0\\ 0 & h\neq 0\end{cases} \qquad \text{Eq. 17}$$

is the indicator function.

Note that the coregionalization matrices after computation from the Goulard-Voltz algorithm are normalized as:

$$\frac{P_{ij}^l}{\sqrt{P_{ii}^1+P_{ii}^2+P_{ii}^3}+\sqrt{P_{jj}^1+P_{jj}^2+P_{jj}^3}}\ . \qquad \text{Eq. 18}$$

Inclusion of Frequency-Dependent Spatial Correlation into Ground Motion Simulation

We demonstrate and validate our spatial correlation approach on the San Diego State University Broadband Ground Motion Generation Module (hereafter the "SDSU Module") (Olsen and Takedatsu, 2015; Mai *et al.*, 2010; Mena *et al.*, 2010).

Our implementation approach for the frequency-dependent spatial correlation is an extension of that developed by Wang et al. (2019) for incorporating inter-frequency correlation. The spatial correlation model in Equation 16 is developed for the within-event residual of the orientation-independent EAS, while the SDSU Module simulations generate separate components of ground

motion. For this reason, we apply the EAS frequency-dependent spatial correlation model to the FAS of each of the two horizontal components generated by the method. The resulting synthetic time histories are then found to include correlations in agreement with the EAS model, provided the FAS adjustments made to the two individual horizontal components at each station are suitably correlated. We use a correlation coefficient of 0.7 for the two FAS component adjustments at the same station, a value recommended by Wang et al. (2019) from their study on inter-frequency correlation.

We illustrate our method using 50 source realizations for the Loma Prieta earthquake obtained by the kinematic source generator module by Graves and Pitarka (2015). Figure 1 (bottom) shows the spatial correlation coefficients of EAS from 50 source realizations of the Loma Prieta earthquake generated from the SDSU Module with the implementation of our spatial correlation method, at example frequency pairs. It can be seen that, without the spatial correlation implementation step, the synthetics show almost zero interstation correlation (typically less than 0.1 for any frequency pair) for separation distances exceeding a kilometer or two. In contrast, the correlation implementation step results in correlation of the synthetics that very closely follows the empirical model, with significant correlation persisting to distances of ~50 km. The correlation has subtle effects on the time domain.

The fact that the SDSU Module correlation implementation allows the correlated synthetics to essentially replicate the empirical correlation for PSA suggests that one could now use the correlated SDSU Module synthetics (with the present EAS model implemented) to generate any other ground motion metrics with a valid "empirical" correlation, such as Arias intensity and Cumulative Absolute Velocity. This also suggests that the correlated SDSU Module synthetics may provide a means for deriving correlation models for other ground motion metrics.

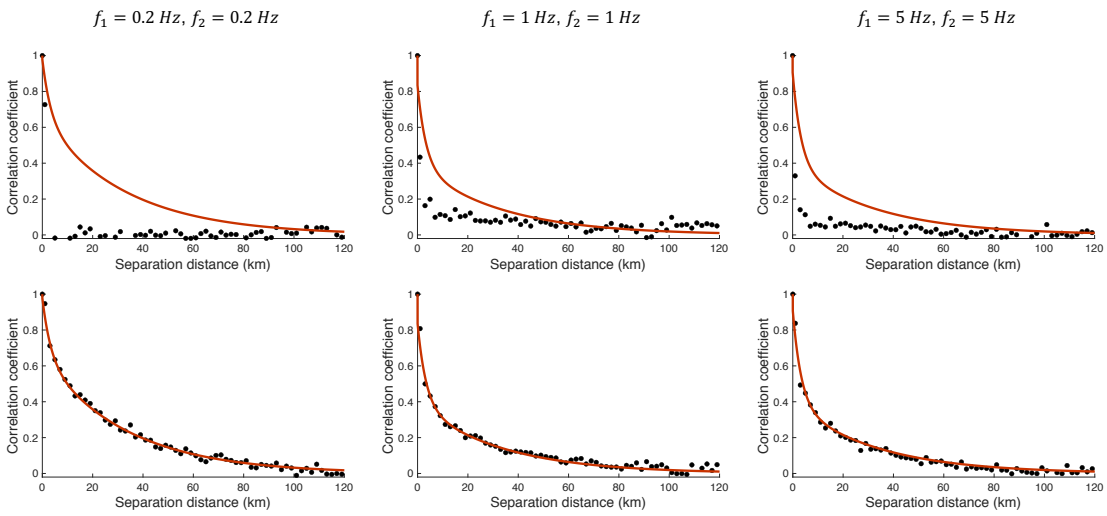

Figure 1. Comparison of the spatial correlation coefficients of epsilon for EAS at the reference frequency pairs $f_1 = f_2 = 0.2\ Hz$ (left), $f_1 = f_2 = 1\ Hz$ (middle) and $f_1 = f_2 = 5\ Hz$ (right) from the proposed model (red lines) and the SDSU Module before (top) and after (bottom) applying our method (dots) for the Loma Prieta earthquake with 50 source realizations.

References

ABRAHAMSON, N. A., SILVA, W. J. & KAMAI, R., 2014. SUMMARY OF THE ASK14 GROUND MOTION RELATION FOR ACTIVE CRUSTAL REGIONS. *EARTHQUAKE SPECTRA,* 30(3), PP. 1025-1055.

Abrahamson, N., Schneider, J. & Stepp, J., 1991. Spatial coherency of shear waves from the Lotung, Taiwan large-scale seismic test. *Structural Safety,* 10(1-3), pp. 145-162.

Al Atik, L. et al., 2010. The variability of ground-motion prediction models and its components. *Seismological Research Letters,* 81(5), pp. 794-801.

Ancheta, T. et al., 2014. NGA-West2 database. *Earthquake Spectra,* 30(3), pp. 989-1005.

Atkinson, G. M. & Assatourians, K., 2015. Implementation and validation of EXSIM (a stochastic finite-fault ground-motion simulation algorithm) on the SCEC broadband platform. *Seismological Research Letters,* 86(1), pp. 48-60.

Atkinson, G. M. et al., 2009. A guide to differences between stochastic point-source and stochastic finite-fault simulations. *Bulletin of the Seismological Society of America,* 99(6), pp. 3192-3201.

Bayless, J. & Abrahamson, N. A., 2018a. Evaluation of the inter-period correlation of ground motion simulations. *Bulletin of the Seismological Society of America,* 108(6), pp. 3413-3430.

Bayless, J. & Abrahamson, N. A., 2018b. *An empirical model for Fourier amplitude spectra using the NGA-West2 database,* University of California, Berkeley, CA: Pacific Earthquake Engineering Research Center.

Beresnev, I. A. & Atkinson, G. M., 1997. Modeling finite-fault radiation from the ω^n spectrum. *Bulletin of the Seismological Society of America,* 87(1), pp. 67-84.

Bolt, B. et al., 1982. *Preliminary report on the SMART-1 strong motion array in Taiwan,* s.l.: Earthquake Engineering Research Center Report.

Boore, D. et al., 2003. Estimated ground motion from the 1994 Northridge, California, earthquake at the site of the Interstate 10 and La Cienega Boulevard bridge collapse, West Los Angeles, California. *Bulletin of the Seismological Society of America,* 93(6), pp. 2737-2751.

Boore, D. M., 2003. Simulation of ground motion using the stochastic method. *Pure and applied geophysics,* 160(3-4), pp. 635-676.

Boore, D. M., 2009. Boore, D.M., 2009. Comparing stochastic point-source and finite-source ground-motion simulations: SMSIM and EXSIM. *Bulletin of the Seismological Society of America,* 99(6), pp. 3202-3216.

Bycroft, G., 1980. *El Centro, California, differential ground motion array,* s.l.: US Geological Survey.

Crempien, J. G. & Archuleta, R. J., 2015. UCSB method for simulation of broadband ground motion from kinematic earthquake sources. *Seismological Research Letters,* 86(1), pp. 61-67.

Dreger, D. S. et al., 2015. Validation of the SCEC Broadband Platform V14.3 Simulation Methods Using Pseudospectral Acceleration Data. *Seismological Research Letters,* 86(1), pp. 39-47.

Esposito, S. & Iervolino, I., 2011. PGA and PGV spatial correlation models based on European multievent datasets. *Bulletin of the Seismological Society of America,* 101(5), pp. 2532-2541.

Goda, K. & Hong, H., 2008. Spatial correlation of peak ground motions and response spectra. *Bulletin of the Seismological Society of America,* 98(1), pp. 354-365.

Goulard, M. & Voltz, M., 1992. Linear coregionalization model: tools for estimation and choice of cross-variogram matrix. *Mathematical Geology,* 24(3), pp. 269-286.

Goulet, C., Abrahamson, N., Somerville, P. & Wooddell, K., 2015. The SCEC Broadband Platform validation exercise for pseudo-spectral acceleration: Methodology for code validation in the context of seismic hazard analyses. *Seismological Research Letters,* 86(1).

Goulet, C. A. et al., 2018. *Effective amplitude spectrum (EAS) as a metric for ground motion modeling using Fourier amplitudes.* Miami, Florida, 2018 Seismology of the Americas Meeting.

Graves, R. & Pitarka, A., 2015. Refinements to the Graves and Pitarka (2010) broadband ground-motion simulation method. *Seismological Research Letters,* 86(1), pp. 75-80.

Hao, H., Oliveira, C. & Penzien, J., 1989. Multiple-station ground motion processing and simulation based on SMART-1 array data. *Nuclear Engineering and Design,* 111(3), pp. 293-310.

Harichandran, R. & Vanmarcke, E., 1986. Stochastic variation of earthquake ground motion in space and time. *Journal of Engineering Mechanics,* 112(2), pp. 154-174.

Heresi, P. & Miranda, E., 2019. Uncertainty in intraevent spatial correlation of elastic pseudo-acceleration spectral ordinates. *Bulletin of Earthquake Engineering,* 17(3), pp. 1099-1115.

Hole, J. A., 1992. Nonlinear high-resolution three-dimensional seismic travel time tomography. *Journal of Geophysical Research: Solid Earth,* 97(B5), pp. 6553-6562.

Jayaram, N. & Baker, J., 2009. Correlation model for spatially distributed ground-motion intensities. *Earthquake Engineering & Structural Dynamics,* 38(15), pp. 1687-1708.

Jayaram, N. & Baker, J. W., 2010. Efficient sampling and data reduction techniques for probabilistic seismic lifeline risk assessment. *Earthquake Engineering & Structural Dynamics,* 39(10), pp. 1109-1131.

Kawakami, H. & Mogi, H., 2003. Analyzing spatial intraevent variability of peak ground accelerations as a function of separation distance. *Bulletin of the Seismological Society of America,* 93(3), pp. 1079-1090.

Kiureghian, A., 1996. A coherency model for spatially varying ground motions. *Earthquake Engineering & Structural Dynamics,* 25(1), pp. 99-111.

Konno, K. & Ohmachi, T., 1998. Ground-motion characteristics estimated from spectral ratio between horizontal and vertical components of microtremor. *Bulletin of the Seismological Society of America,* 88(1), pp. 228-241.

Kottke, A. et al., 2018. Selection of Random Vibration Procedures for the NGA-East Project. *PEER report.*

Loth, C. & Baker, J. W., 2013. Loth, C. and Baker, J.W., 2013. A spatial cross-correlation model of spectral accelerations at multiple periods. *Earthquake Engineering & Structural Dynamics,* 42(3), pp. 397-417.

Mai, P. M., Imperatori, W. & Olsen, K. B., 2010. Hybrid broadband ground-motion simulations: Combining long-period deterministic synthetics with high-frequency multiple S-to-S backscattering. *Bulletin of the Seismological Society of America,* 100(5A), pp. 2124-2142.

Markhvida, M., Ceferino, L. & Baker, J. W., 2018. Modeling spatially correlated spectral accelerations at multiple periods using principal component analysis and geostatistics. *Earthquake Engineering & Structural Dynamics,* 47(5), pp. 1107-1123.

Mena, B. et al., 2010. Hybrid broadband ground-motion simulation using scattering Green's functions: Application to large-magnitude events. *Bulletin of the Seismological Society of America,* 100(5A), pp. 2143-2162.

Miller, M. & Baker, J., 2015. Ground-motion intensity and damage map selection for probabilistic infrastructure network risk assessment using optimization. *Earthquake Engineering & Structural Dynamics,* 44(7), pp. 1139-1156.

Motazedian, D. a. G. M. A., 2005. Stochastic finite-fault modeling based on a dynamic corner frequency. *Bulletin of the Seismological Society of America,* 95(3), pp. 995-1010.

Olsen, K. B. & Takedatsu, R., 2015. The SDSU broadband ground-motion generation module BBtoolbox version 1.5. *Seismological Research Letters,* 86(1), pp. 81-88.

Sokolov, V., Wenzel, F., Wen, K.-L. & Jean, W.-Y., 2012. Sokolov, V., Wenzel, F., Wen, K.L. and Jean, W.Y., 2012. On the influence of site conditions and earthquake magnitude on ground-motion within-earthquake correlation: analysis of PGA data from TSMIP (Taiwan) network. *Bulletin of Earthquake Engineering,* 10(5), pp. 1401-1429.

Stafford, P. J. (2017). Interfrequency correlations among Fourier spectral ordinates and implications for stochastic ground-motion simulation. *Bulletin of the Seismological Society of America, 107*(6), 2774-2791.

Travasarou, T., Bray J. D. & Abrahamson, N. A., 2003. Empirical attenuation relationship for Arias intensity. *Earthquake Engineering and Structural Dynamics,* 32, pp. 1133-1155.

Wang, M. & Takada, T., 2005. Macrospatial correlation model of seismic ground motions. *Earthquake spectra,* 21(4), pp. 1137-1156.

Wang, N., Takedatsu, R., Olsen, K. B. & Day, S. M., 2019. Broadband Ground-Motion Simulation with Interfrequency Correlations. Bulletin of the Seismological Society of America, 109(6), pp. 2437-2446.

Withers, K. B., Olsen, K. B., Day, S. M., & Shi, Z. (2019). Validation of Deterministic Broadband Ground Motion and Variability from Dynamic Rupture Simulations of Buried Thrust Earthquakes. *Bulletin of the Seismological Society of America*, 109(1), 212-228.

Wesson, R. & Perkins, D., 2001. Spatial correlation of probabilistic earthquake ground motion and loss. *Bulletin of the Seismological Society of America,* 91(6), pp. 1498-1515.

Zeng, Y., Aki, K. & Teng, T., 1993. Mapping of the high-frequency source radiation for the Loma Prieta earthquake, California. *Journal of Geophysical Research: Solid Earth,* 98(B7), pp. 11981-11993.

Zeng, Y., Su, F. & Aki, K., 1991. Scattering wave energy propagation in a random isotropic scattering medium: 1. Theory. *Journal of Geophysical Research: Solid Earth,* 96(B1), pp. 607-619.